Supplementary Information

SARS-CoV-2 Spike protein N501Y mutation causes differential species transmissibility and antibody sensitivity

Xudong Hou[a,b], Zhilin Zhang[b], Jiali Gao[a,b,c], Yingjie Wang[b*]

[a]*College of Chemical Biology and Biotechnology, Peking University Shenzhen Graduate School, Shenzhen, 518055, China*
[b]*Institute of Systems and Physical Biology, Shenzhen Bay Laboratory, Shenzhen, 518132, China*
[c]*Department of Chemistry and Supercomputing Institute, University of Minnesota, Minneapolis, MN 55455, USA*

*Corresponding Author

Yingjie Wang: wangyj@szbl.ac.cn; +86-18310827828

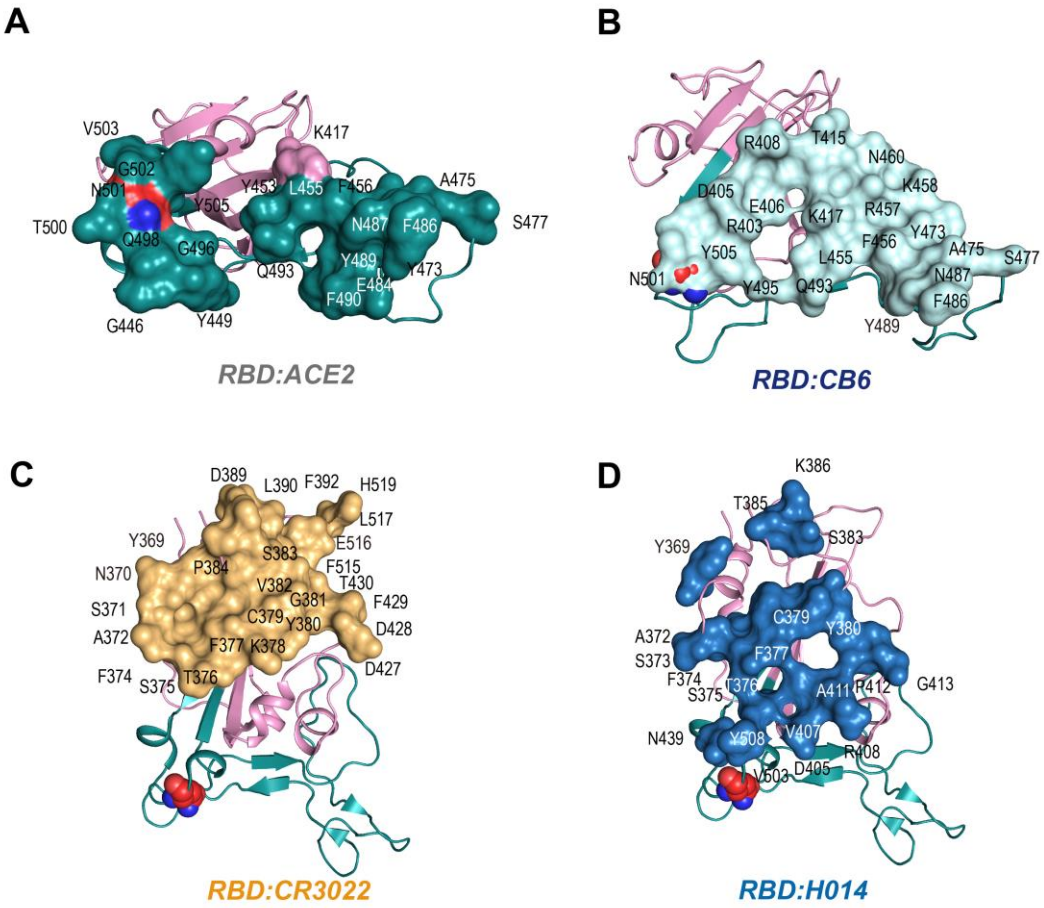

Figure S1. The structural epitopes on RBD for hACE2 and antibodies. (A). Epitopes for hACE2 primiarly locate at RBM, with N501 is at the center of contact surface. (B). Epitopes for CB6 also locate at RBM, whereas N501 is at the boundary of contact surface. (C). Epitopes of CR3022 primarily locate at the core region, distant from N501. (D). Epitopes of H014 span both the core and part of RBM, with N501 in proximity to the contact surface.

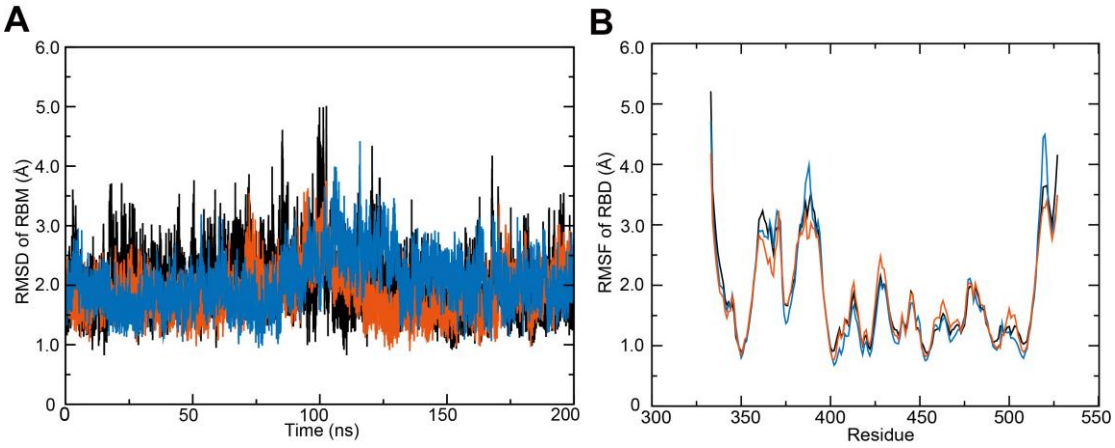

Figure S2. Convergence of the (A) RMSD and (B) RMSF for triplicate simulations of RBD^{WT}:hACE2, where the three trajectories are colored by black, orange and blue respectively.

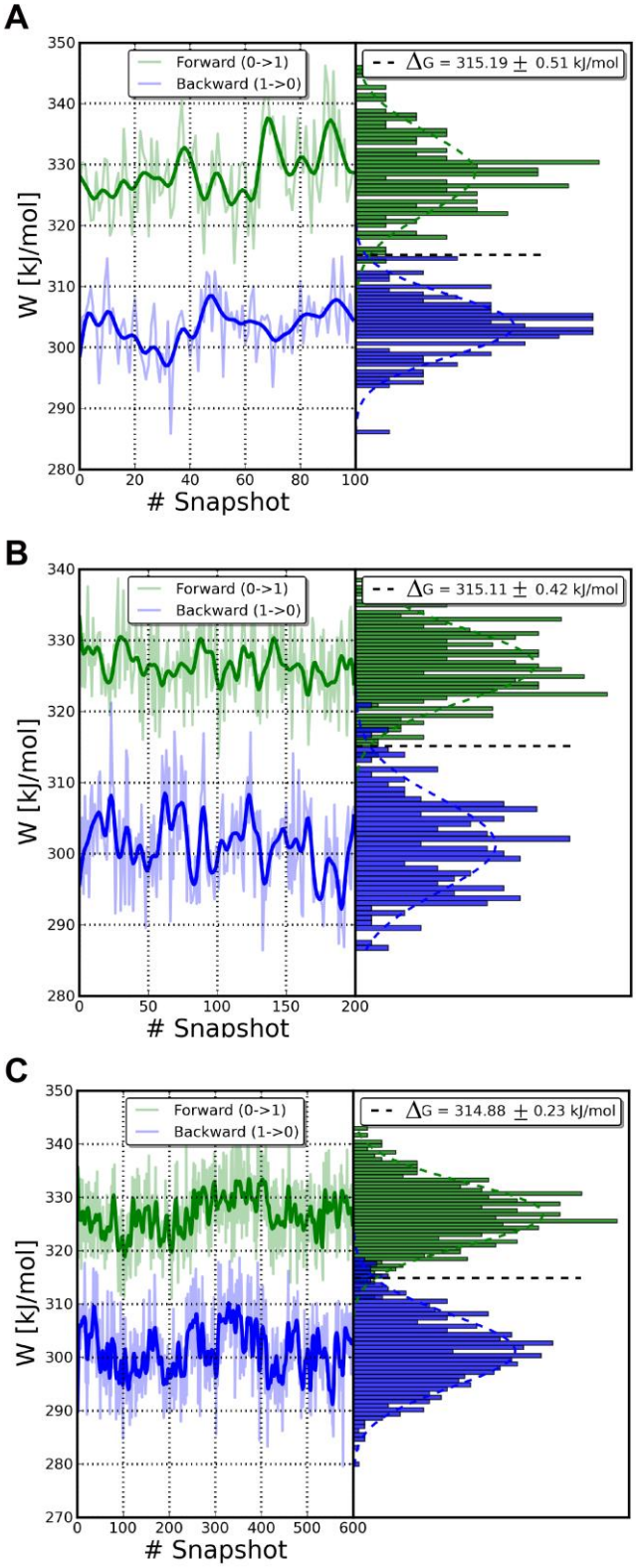

Figure S3. Convergence of ΔG_{apo} with different settings for non-equilibrium free energy calculation. (A) 20 ns equilibration each for the end states ($\lambda = 0$ and $\lambda = 1$), followed by 100 non-equilibrium forward and backward transitions, respectively. (B) 40 ns equilibration, 200 non-equilibrium transitions. (C) 100 ns equilibration, 600 non-equilibrium transitions.

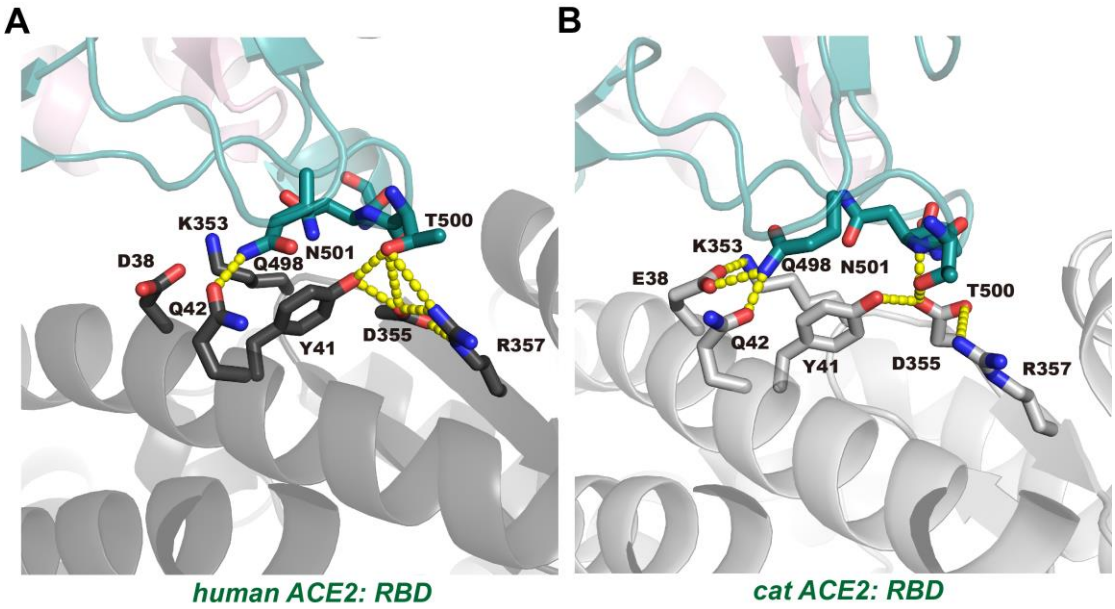

Figure S4. Comparison of local interaction network between (A) hACE2:RBD and (B) cACE2:RBD, highlighting different orientations of D355 and N501, as well as the more crowded packing in the cACE2:RBD complex. Note that the amino acid change from D38 in hACE2 to E38 in cACE2 strengthens the local hydrogen bond network, thus making CR3 of cACE2:RBD complex more compact.

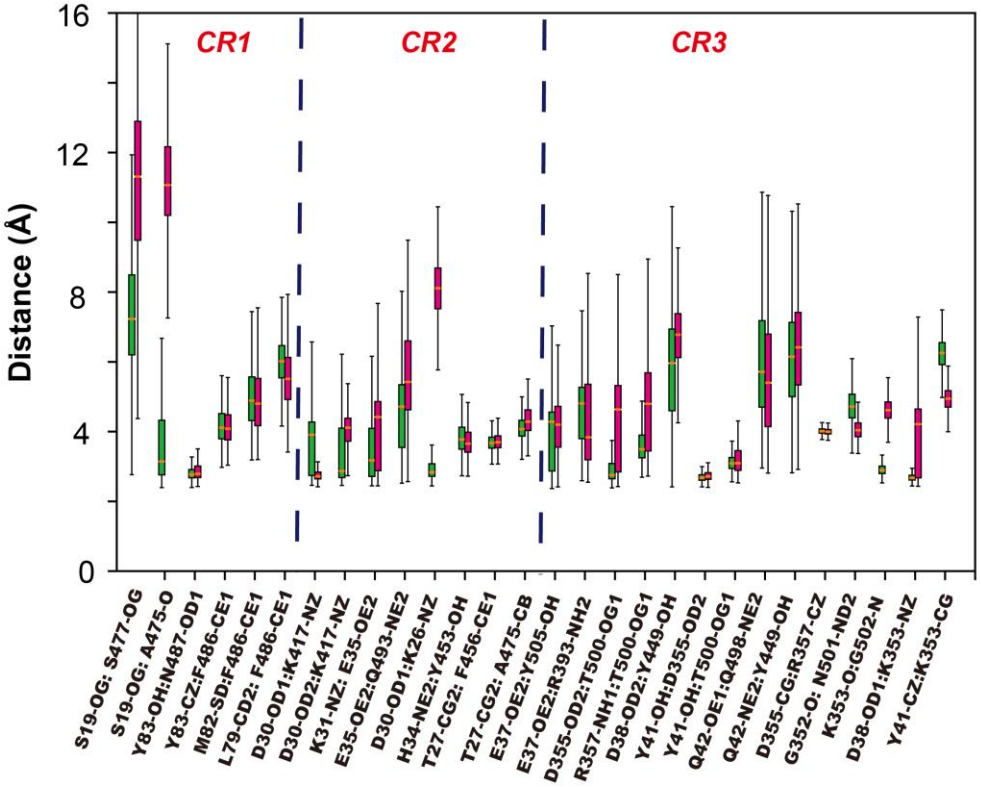

Figure S5. Comparison of distance distribution of interacting residue pairs at contact interface for RBD^{WT}:hACE2 and RBD^{N501Y}:hACE2, highlighting preservation of major interactions from CR1 to CR3.

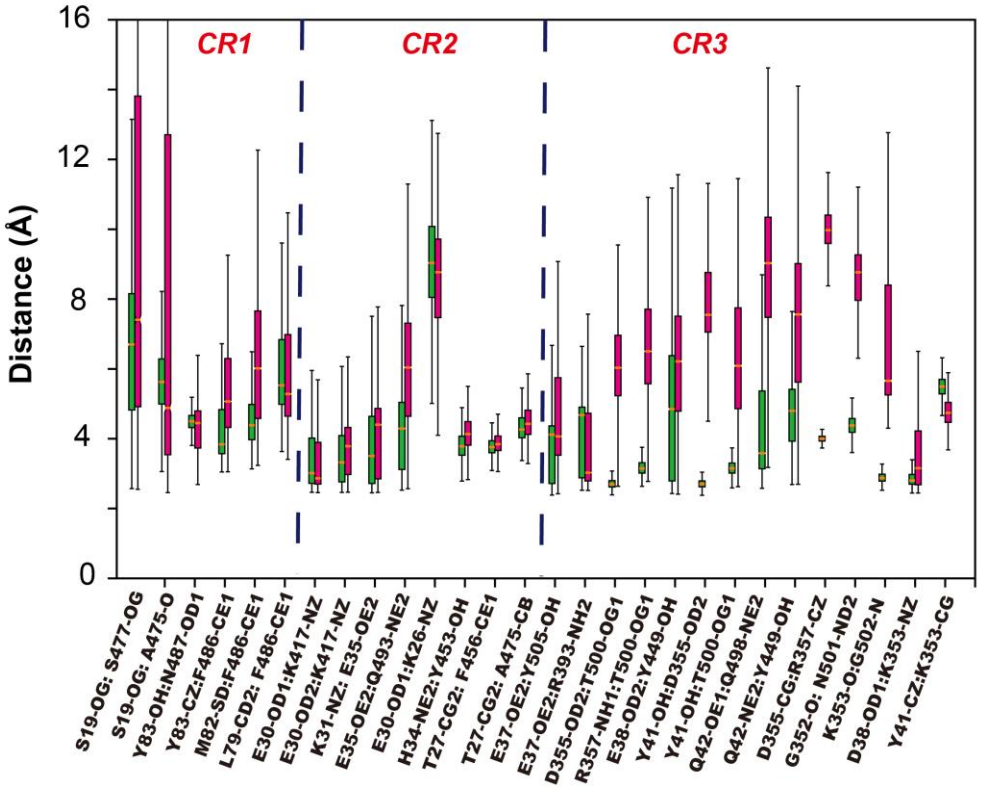

Figure S6. Comparison of distance distribution of interacting residue pairs at contact interface for RBD^{WT}:cACE2 and RBD^{N501Y}:cACE2, highlighting preservation of major interactions in CR1 and CR2, yet the disruption of hydrogen bonding networks in CR3.

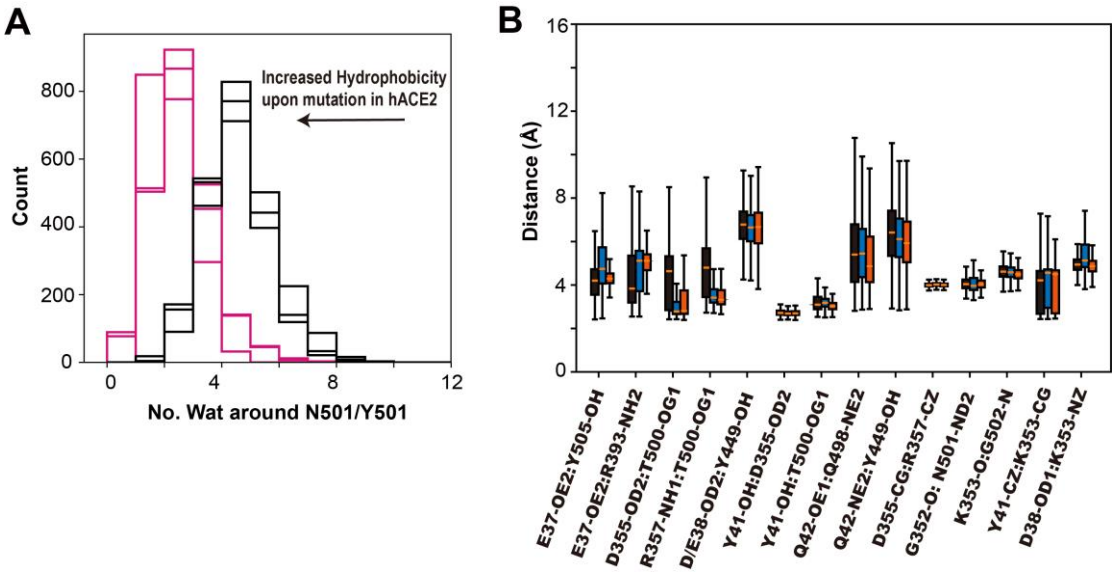

Figure S7. Convergence of the local interaction in the CR3 region in triplicate trajectories. (A) Three sets of histograms of water molecules around N501/Y501 are plotted for both WT (black) and mutant (magenta), respectively, highlighting a converged pattern of increased hydrophobicity upon N501Y mutation. (B) The distance distribution of key interaction pairs in CR3 for the triplicate simulations of RBD^{N501Y}:hACE2.

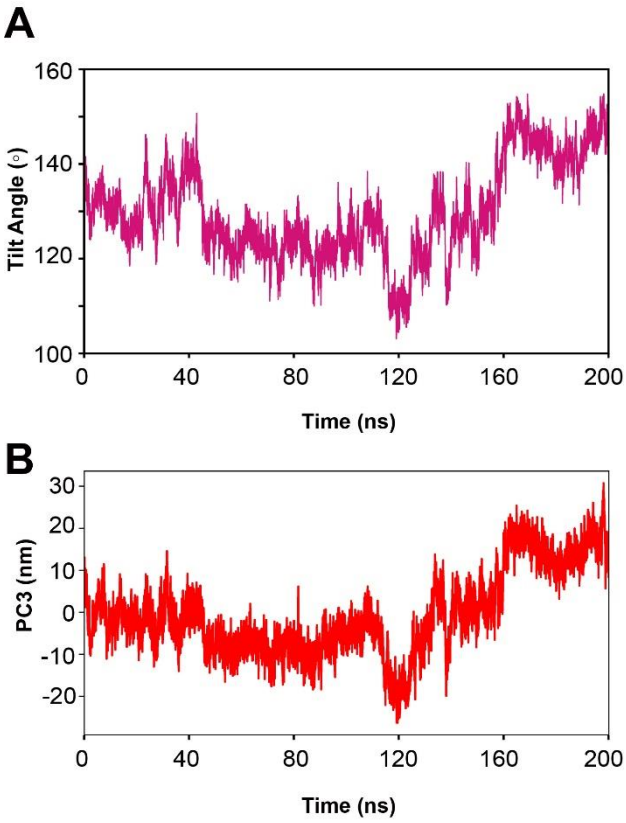

Figure S8. Coincidence between (A) the tilt angle and (B) projection on PC3 for RBD^{N501Y}: cACE2 complexes, suggesting that the two motion modes are highly correlated.